Check for updates

A quantitative *ex vivo* study of the interactions between reconstituted high-density lipoproteins and human leukocytes†

Dennis Pedersbæk, [iD] [a] Katrine Jønsson, [iD] [a] Ditte V. Madsen,[a] Sven Weller, [iD] [a] Anja B. Bohn,[b] Thomas L. Andresen[a] and Jens B. Simonsen [iD] *[a]

Knowledge of the interactions between nanoparticles and immune cells is required for optimal design of nanoparticle-based drug delivery systems, either when aiming to avoid phagocytic clearance of the nanoparticles or promote an immune response by delivering therapeutic agents to specific immune cells. Several studies have suggested that reconstituted high-density lipoproteins (rHDL) are attractive drug delivery vehicles. However, detailed studies of rHDL interactions with circulating leukocytes are limited. Here, we evaluated the association of discoidal rHDL with leukocytes in human whole blood (HWB) using quantitative approaches. We found that while the rHDL of various lipid compositions associated preferentially with monocytes, the degree of association depended on the lipid composition. However, consistent with the long circulation half-life of rHDL, we show that only a minor fraction of the rHDL associated with the leukocytes. Furthermore, we used three-dimensional fluorescence microscopy and imaging flow cytometry to evaluate the possible internalization of rHDL cargo into the cells, and we show increased internalization of rHDL cargo in monocytes relative to granulocytes. The preferential rHDL association with monocytes and the internalization of rHDL cargo could possibly be mediated by the scavenger receptor class B type 1 (SR-BI), which we show is expressed to a higher extent on monocytes than on the other major leukocyte populations. Our work implies that drug-loaded rHDL can deliver its cargo to monocytes in circulation, which could lead to some off-target effects when using rHDL for systemic drug delivery, or it could pave the way for novel immunotherapeutic treatments aiming to target the monocytes.

Introduction

It is widely acknowledged that the influence of the immune system must be considered when designing novel nanoparticle-based drug delivery systems, either to avoid clearance of the carriers or to target specific immune cells for immuno-therapy.[1–3] Several drug delivery systems aim to target tumors by the enhanced permeability and retention (EPR) effect, where limited interactions between the nanoparticles and the leukocytes are desired, *e.g.* by grafting polyethylene glycol onto the surface of liposomes.[4] Contrarily, instead of avoiding interactions with the immune system, several immunotherapeutic strategies involve targeting specific immune cells.[1,5] These strategies include, amongst many others, the delivery of cancer antigens and adjuvants to dendritic cells (DCs) for treatment of

cancer[6] and the depletion of macrophages at atherosclerotic plaque sites for treating atherosclerosis.[7]

Many of the immunotherapeutic strategies aim to target DCs,[6,8] macrophages[7,9] or T-cells,[10] however, another less explored method is to target circulatory monocytes.[11] As monocytes can differentiate into both macrophages and DCs,[12] delivering therapeutic agents directly to monocytes can potentially facilitate the initiation or inhibition of an immune response before the monocyte differentiate. Delivering therapeutics to monocytes has been used both as an approach for anticancer immunotherapy relying on activation of the monocytes[11] as well as an approach for treatment of atherosclerosis relying on silencing the receptors responsible for recruitment of the monocytes to the atherosclerotic plaque.[13] Furthermore, depletion of monocytes has also been shown to be advantageous for inflammatory diseases.[14–16] However, when developing therapies based on systemic targeting of monocytes, one has to be aware of the potential side-effects of affecting an entire leukocyte population. For example, depleting the monocytes or limiting their recruitment to inflammatory sites would obviously disrupt the normal function of the monocytes, which is essential for protection against infections.[12,17] Hence, while the

[a]Department of Health Technology, Technical University of Denmark, 2800 Kongens Lyngby, Denmark. E-mail: jbak@dtu.dk

[b]Department of Biomedicine, Aarhus University, 8000 Aarhus, Denmark

† Electronic supplementary information (ESI) available. See DOI: 10.1039/c9ra08203d

Paper

association of drug-carrying nanoparticles with monocytes both can cause positive and negative therapeutic effects, in either case, the characterization of the potential association is essential.

The uptake of particles in phagocytic cells, including monocytes, has been found to be highly dependent on charge with the preferential uptake of highly anionic particles.[18,19] Therefore, modification of the particle surface charge has been used in several studies to achieve monocyte specificity. Johansen *et al.*[11] used a liposome formulation with an incorporated toll-like receptor (TLR) agonist. They were able to obtain specific monocyte association by modifying the charge on the lipid bilayer. While they found no monocyte specificity for neutral or slightly anionic charged liposomes, they found that liposomes containing 10% cationic lipids had high monocyte specificity, thus allowing for specific drug delivery to the monocytes.

As charged liposomes have intrinsic monocyte specificity,[11,16] this specificity may also apply to other lipid-based particles. Furthermore, even though Johansen *et al.*[11] showed no cytotoxicity of their cationic liposomes, it is well-established that cationic lipids can explicit toxicity,[20] hence, testing other types of particles for monocyte-targeting applications is indeed relevant. Reconstituted high-density lipoproteins (rHDL) are another class of lipid-based nanoparticles, which have recently been shown to be promising drug delivery vehicles, both for applications that aim to target specific immune cells and for applications that aim to avoid recognition by the immune system.[21-23] The rHDL mimic the endogenous HDL, which are involved in the transport and metabolism of lipids in circulation.[24,25] The HDL are also known to have anti-inflammatory properties, *e.g.* by binding proteins and lipids with immunomodulatory activities, such as lipopolysaccharides (LPS), and by modulating receptor expression and differentiation of several types of leukocytes.[26] The HDL and rHDL can have both discoidal and spherical morphology, but the vast majority of studies applying rHDL for drug delivery focus on the discoidal rHDL (Fig. 1) consisting of a lipid bilayer stabilized at the edges by apolipoproteins, *e.g.* apolipoprotein A-I (apoA-I), or peptides.[24] The discoidal rHDL (with apoA-I) will also be the focus of this study (hereafter referred to merely as rHDL). The rHDL can utilize several of the properties of HDL, including high biocompatibility and biodegradability as well as possible recognition by endogenous receptors that facilitate uptake of rHDL cargo into the cells.[24,25] One of the most relevant HDL receptors is the scavenger receptor class B type 1 (SR-BI), which mediates cholesterol flux between HDL and cells.[27] As the SR-BI is expressed on monocytes (though weakly),[28,29] it can potentially facilitate interactions between the rHDL and the monocytes. While the presence of apoA-I is essential for the binding of HDL/rHDL to SR-BI,[27,30] it has also been found that this scavenger receptor can recognize anionic phospholipids,[31] thus, the rHDL interaction with SR-BI is potentially affected by the rHDL composition.

Although, it has been shown that rHDL with different sizes and morphologies can associate with monocytes, DCs and neutrophils,[32] a thorough study is needed to establish the effect of rHDL lipid composition, including charge, where the rHDL
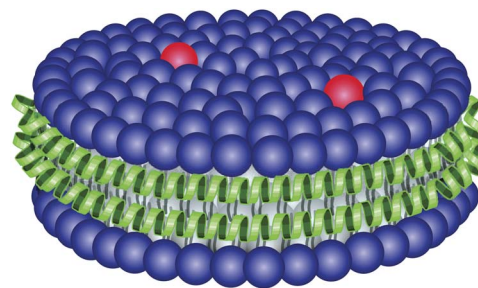

Fig. 1 Illustration of the discoidal rHDL particle. It is ~10 nm in diameter and consists of a lipid bilayer (blue) containing lipid-conjugated fluorophores (red), which is stabilized at the edges by two apoA-I apolipoproteins (green).

association with monocytes is compared more quantitatively to the other major leukocyte populations in blood (granulocytes and lymphocytes) – also taken the different number of each cell into account. Furthermore, a detailed study of the association and potential uptake of rHDL cargo into the cells is also needed to fully understand the rHDL association with leukocytes.

We used a simple approach to quantify the amount of rHDL associated with the blood cells, showing that only a minor amount of the rHDL associated with the blood cells after four hours of incubation (~15%), which is consistent with the relatively long circulation half-life of rHDL. Using flow cytometry, we show that the rHDL that do associate with the leukocytes preferentially associate with monocytes over granulocytes and lymphocytes. Interestingly, the preferred monocyte association seems to be largely independent of the lipid composition and charge of the rHDL in contrast to liposomes. However, we did find that the degree of association was affected by the rHDL compositional design, thus allowing for possible maximization or minimization of rHDL association with monocytes. We show that SR-BI is expressed more on monocytes than the other major leukocyte populations, thus, it is likely involved in the observed preferential monocyte association of rHDL. Although the rHDL associated preferentially with monocytes, we used a novel quantitative approach to show that the leukocyte-associated rHDL are distributed approximately equally between granulocytes and monocytes, which can be explained by the relative higher abundance of granulocytes that associate with a minor amount of rHDL. Furthermore, we used three-dimensional fluorescence microscopy and imaging flow cytometry to determine the internalization of rHDL cargo into the cells, and we observed increased internalization in monocytes compared to granulocytes. Overall, we used quantitative methods to reveal essential aspects of rHDL interactions with leukocytes which are important for any kind of rHDL based drug delivery applications.

Experimental

Materials

The phospholipids 1,2-dipalmitoyl-*sn-glycero*-3-phosphocholine (DPPC), 1,2-dimyristoyl-*sn-glycero*-3-phosphocholine (DMPC), 1-

palmitoyl-2-oleoyl-*glycero*-3-phosphocholine (POPC) and 1,2-dipalmitoyl-*sn*-*glycero*-3-phospho-(1′-*rac*-glycerol) (DPPG) were all supplied from Avanti Polar Lipids (USA). The fluorophores 3,3′-dioctadecyloxacarbocyanine (DiO) and 1,1′-dioctadecyl-3,3,3′,3′-tetramethylindotricarbocyanine iodide (DiR) as well as RIPA Lysis and Extraction buffer and Hoechst were obtained from ThermoFisher Scientific (USA). BD Pharm Lyse™ lysing solution, anti-CD14 antibody (APC Mouse Anti-Human CD14, IgG2a, κ, Clone M5E2) and CD14 isotype control (APC Mouse IgG2a, κ Isotype Control, Clone G155-178) were supplied by BD Biosciences (USA). Anti-CD14 antibody (APC Mouse Anti-Human CD14, IgG1, κ, Clone 61D3) used for imaging flow cytometry was supplied by ThermoFisher Scientific (USA). The anti-SR-BI antibody (PE Mouse Anti-Human CD36L1 (SCARB1, SR-BI), Clone m1B9) and isotype control (PE Mouse IgG1, κ) used for SR-BI staining was supplied by Biolegend (USA).

RPMI, *tert*-butanol, Phosphate Buffered Saline (PBS), Fetal Bovine Serum (FBS) and human IgG were all supplied from Sigma Aldrich (Denmark). The human whole blood (HWB) was obtained from healthy volunteers (according to DTU guidelines that includes protection of the donor and the researchers) and collected in Hirudin blood tubes from Roche Diagnostics (Austria).

Preparation of rHDL

The rHDL were prepared using the detergent depletion method using apoA-I purified from human plasma (purity > 99%). The purification of apoA-I from human plasma was conducted similarly to what has been described elsewhere.[33] The rHDL were prepared by first freeze-drying a solution of the phospholipids and the fluorophore (1 mol%) dissolved in a *tert*-butanol:MilliQ 9:1 solution. Subsequently, the lipids were rehydrated in a PBS solution containing apoA-I and 20 mM sodium cholate yielding a lipid concentration of 5 mM, and a lipid:protein molar ratio of ∼100:1 when using DPPC, DPPG and DMPC and 90:1 when using POPC. Bio-Beads™ SM-2 from Bio-Rad (Denmark) were mixed with the solution using 0.6 μg Bio-Beads per μL of solution in order to deplete the detergent and induce self-assembly of rHDL. The samples were incubated with the Bio-Beads overnight at 41 °C for DPPC and DPPG rHDL, 24 °C for DMPC rHDL and 4 °C for POPC rHDL, before separating the Bio-Beads from the solution. The rHDL were characterized with size-exclusion chromatography (SEC) using a Superdex 200 Increase 10/300 GL (GE Healthcare) column on a HPLC system from Shimadzu (a LC-20AD pump, a DGU-20A SR degassing unit, a SIL-20AC HT autosampler, a SPD-M20A Photodiode Array (PDA) Detector and a FRC-10A fraction collector). Furthermore, the rHDL size was confirmed with dynamic light scattering (DLS) using a ZetaSizer Nano ZS from Malvern Instruments.

Studying the degree of rHDL association with leukocytes

In order to quantify the degree of rHDL association with cells in HWB, DPPC rHDL, containing 1 mol% of the fluorophore DiR, were initially incubated in HWB (0.1 mM rHDL lipid in 400 μL HWB), after which the plasma and cells were separated by centrifugation (2000g for 15 min). Some of the supernatant (100 μL) was removed, diluted 1:9 in RIPA buffer and incubated overnight at 37 °C, before measuring fluorescence from DiR using a TECAN Spark microplate reader (TECAN) with excitation wavelength of 710(5) nm and emission wavelength of 800(10) nm. The degree of association with the blood cells was determined by the decrease in fluorescence signal relative to a control rHDL sample (diluted 1:9 in RIPA) containing the same amount rHDL as applied to the HWB (using the assumption that the HWB consists of 50 vol% plasma and 50 vol% cells).

Studying rHDL association with leukocytes

The rHDL solution was diluted 1:1 in RPMI yielding a 2.5 mM lipid concentration. This solution was further diluted 1:4 in HWB and subsequently incubated for 1 hour at 37 °C. After washing the cells twice with PBS + 1% FBS, the erythrocytes were lysed with BD Pharm Lyse™ lysing solution using 5 mL of the 10× diluted lysing solution for 200 μL HWB. The samples were initially incubated for 15 minutes, after which the lysis buffer was replaced with fresh lysis buffer, and incubated for an additional 5 minutes. Subsequently, the cells were washed twice and IgG solution (2 μg IgG per million cells) was added to block unspecific binding of antibodies. CD14 antibodies (10 μL) were added to each sample and the cells were washed after 30 minutes of incubation on ice. The cells were re-suspended in PBS and analyzed by the Accuri C6 flow cytometer counting 100 000 cells for each sample. Granulocytes and lymphocytes were identified based on a forward scatter *versus* side scatter plot, whereas monocytes were identified based on both the forward scatter *versus* side scatter plot and the CD14 staining (the gating strategy is illustrated in ESI Fig. S1†). The rHDL cargo (DiO) was detected by its fluorescence using an excitation wavelength of 488 nm and collecting emitted light between 518 nm and 548 nm. As the amount of DiO in the rHDL varied slightly, the measured geometric mean fluorescence intensity (MFI) was adjusted with the integral of DiO absorbance (at 484 nm) from the SEC analysis of each rHDL formulation such that the adjusted MFI value from the different rHDL formulations is comparable.

To estimate the distribution of rHDL between the leukocytes, *i.e.* the likelihood of the rHDL to associate to a given type of leukocyte, the following equation was used. It is here exemplified with the distribution of rHDL in monocytes (D_m) – a number between 0 and 1, but calculated similarly for each leukocyte subset:

$$D_m = \frac{N_{m,c}(M_m - M_{m,c})}{N_{m,c}(M_m - M_{m,c}) + N_{g,c}(M_g - M_{g,c}) + N_{l,c}(M_l - M_{l,c})}$$

(1)

where N is the number of cells, and M is the MFI, while the subscripts m, g, l represent monocytes, granulocytes and lymphocytes, respectively. The subscript c refers to the untreated control sample from each donor.

Studying the internalization of rHDL cargo

To study the internalization of rHDL cargo into monocytes qualitatively, we used three-dimensional fluorescence microscopy. The cells were prepared as for conventional flow cytometry, and

stained with CD14 and Hoechst (10 μg mL^{-1}) for 30 minutes on ice, before being transferred to a μ-Slide 8 Well (ibidi GmbH, Germany) and imaged herein using an inverted Nikon Ti2 Spinning Disc confocal microscope. Image processing and 3D-visualization was done using Fiji, a distribution of ImageJ (ver. 1.52p), and Nicon NIS-Element AR (ver. 5.11.00) analysis software.

To further investigate the possible internalization of the rHDL cargo in monocytes and granulocytes more quantitatively and in a high-throughput manner, imaging flow cytometry were conducted using an Amnis Imagestream MK II Imaging Flow Cytometer (Luminex Corporation, USA). For each sample 1000 CD14+ cells were counted and analyzed in the following channels: Ch01 (brightfield), Ch02 (DiO, 480–560 nm) of the 488 nm laser (20 mW), Ch06 (darkfield) of the 785 nm laser (0.5 mW), and Ch11 (anti-CD14 antibody, APC, 640–745 nm) of the 642 nm laser (150 mW). The results were analyzed in IDEAS application v6.2. Both granulocytes and monocytes were identified based on CD14 intensity and intensity in Ch6 (side-scatter/darkfield); (the complete gating strategy is illustrated in ESI Fig. S2†). We used the brightfield images to define the interior of the cell with an eroded object mask, and this mask was used to determine percentage of cells with a high degree of internalized rHDL cargo (DiO) by using the software's internalization feature: Internalization_AdaptiveErode(Object(M01, Ch01 BF, Tight) Ch01 BF, 85)_Ch02 DiO. The internalization feature considers the ratio between the fluorescence intensity within the mask to the intensity from the entire cell. The ratio is adjusted to a log scale (with values between {−Inf, Inf}) such that a value of 0 indicate a mix of internalized particles (fluorophores) and particles (fluorophores) on the surface, and values above 1 indicate that the fluorescence primarily is inside the cell. The gate to define internalized DiO positive cells was defined manually.

SR-BI staining of leukocytes

The leukocytes were obtained from HWB following the same procedure as when studying the association of rHDL with the leukocytes. The SR-BI was stained using a PE-conjugated anti-SR-BI antibody and compared to an isotype control. The anti-SR-BI antibody or isotype control was added (10 μL) to the isolated leukocytes together with the anti-CD14 antibody and incubated for 30 minutes on ice before analysis on Accuri C6 flow cytometer. The granulocytes, lymphocytes and monocytes were identified similarly to when studying the association of rHDL with leukocytes (ESI Fig. S1†).

Results and discussion

Preparation and characterization of the rHDL

The rHDL were prepared using the traditional detergent depletion method,[34] where rHDL self-assembly was induced by depletion of the detergent (cholate) used to dissolve the phospholipids in an aqueous solution containing apoA-I. The detergent was depleted using Bio-Beads™ SM-2. The rHDL samples were characterized with SEC using a Superdex 200 GL 10/300 increase column. The peak around 11–12 mL is characteristic for ~10 nm sized rHDL when analyzed on this

column[33,35,36] (Fig. 2A). The size of the rHDL was also measured by DLS, which confirmed the average size of ~10 nm (Fig. 2B). We have previously characterized similar rHDL in more details.[33] Importantly, all the rHDL formulations used in the present study had similar size and monodispersity according to SEC data (ESI Fig. S3†), thus making it feasible to assess the effect of the lipid composition only.

Degree of rHDL association with leukocytes

It is well-established that rHDL, like the endogenous HDL, have a relatively long circulation half-life,[24] which indicates minimal association between rHDL and leukocytes, however, it is still possible that some of the rHDL do associate with the leukocytes in circulation. We set up a simple experiment to quantify the degree of leukocyte association, where we separated blood cells from plasma by centrifugation. The supernatant was dissolved in RIPA buffer and heated to 37 °C overnight, thereby ensuring disintegration of all plasma aggregates and larger particles, e.g. lipoproteins, and thus keeping the environment around the fluorophores identical. The near-infrared fluorophore DiR was incorporated in the rHDL for these studies to avoid background from autofluorescence. The degree of association with blood cells was determined by the decrease in fluorescence signal relative to a rHDL sample in PBS containing the same amount rHDL as applied to the HWB.

It is evident that less than ~15% of the rHDL are associated with the cells after four hours of incubation (Fig. 3). Notably, these experiments do not distinguish between rHDL associated with leukocytes and erythrocytes, hence, the measured degree of association represent a maximum value for the degree of rHDL association with leukocytes. Though not conclusive due to the relatively large standard error at the measurement at 15 min, there appears to be an increase in the degree of association over the first 60 min, after which it reaches a plateau. We also conducted similar studies, where we used higher concentration of rHDL, and observed similar tendencies though reaching a plateau around ~2% (ESI Fig. S4†), which does indicate saturation of the rHDL association with leukocytes. Consistent with these results, similar saturation of the uptake in leukocytes has previously reported for liposomes.[37] The used ex vivo system is obviously more constricted than in a in vivo setting, where the continuous generation of new monocytes might cause a steadily increase in the degree of leukocyte association, and the quantified ~15% cell association might therefore not be directly comparable. Still, the relatively low degree of rHDL association with leukocytes is consistent with the long circulation half-life of rHDL. Nonetheless, it is relevant to study the association of rHDL with leukocytes in more details as the rHDL that do associate with the leukocytes could result in side-effects from drugs unintentionally delivered to leukocytes in circulation. Alternatively, the rHDL association with leukocytes could pave the way for novel immunotherapeutic strategies, where targeting specific leukocytes are essential, if the drug-loaded rHDL that do not associate with leukocytes are safely cleared.

rHDL association with leukocytes

The association of rHDL with leukocytes was studied by flow cytometry after incubating rHDL with HWB for 1 hour. The
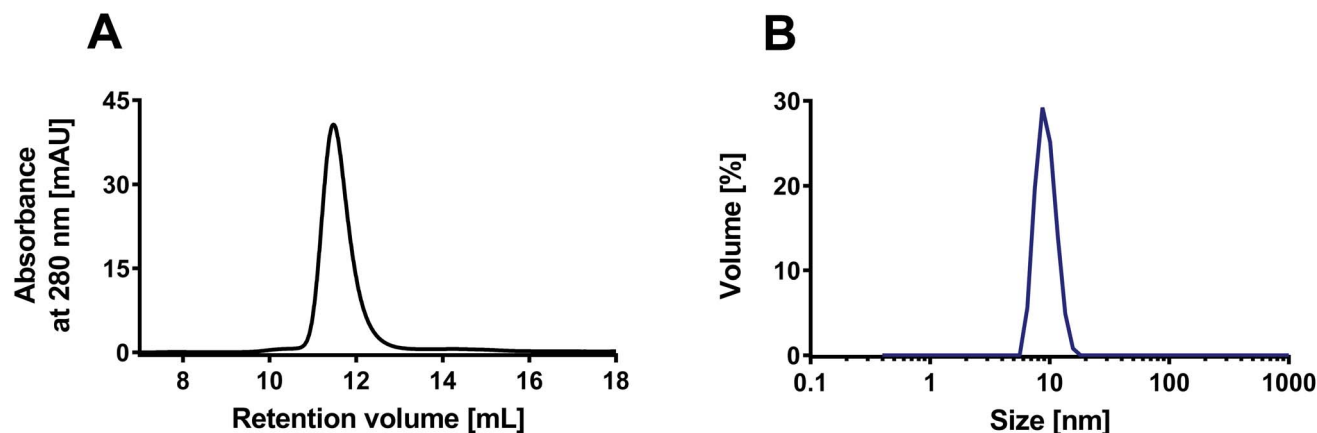
A

B

Fig. 2 Characterization of the rHDL with SEC and DLS. (A) The SEC chromatogram shows elution of the rHDL around 11–12 mL, which is characteristic for ~10 nm sized rHDL. (B) The DLS measurements confirmed the average size of 10 nm. The presented examples represent measurements on DPPC:DiO 99:1 rHDL, but all the used rHDL formulations had similar characteristics (ESI Fig. S3†).

erythrocytes were lysed, after which the rHDL association with the different types of leukocytes could be determined by detection of the fluorophore DiO that had been incorporated into the rHDL. The fluorophore DiO was chosen as it has been shown to be stably incorporated into lipid bilayers,[38,39] including rHDL.[33] We consequently only track the DiO, which represents the rHDL cargo, and even though we are aware that the rHDL can deliver its cargo to cells without uptake of the whole particles,[27] we denote the measured DiO signal as rHDL association with the leukocytes. The leukocytes were divided into three categories: lymphocytes (NK-cells, T-cells and B-cells), granulocytes (primarily neutrophils) and monocytes. Granulocytes and lymphocytes were identified based on their characteristic distribution in a forward scatter *versus* side scatter plot,[40] while the monocytes were identified by first using the forward scatter *versus* side scatter plot and then the CD14 staining.

It has previous been observed that the lipid composition of liposomes significantly influences their leukocyte association.[11] Similar principles might apply for rHDL, hence, we studied the effect of the lipid composition on the association of rHDL with leukocytes by varying both the acyl chain (length and the degree of saturation) and the charge.

Incorporation of cationic lipids (10 mol%) into the rHDL induced instability hereof, since the structural integrity of these rHDL was not preserved after incubation for 8 hours at 37 °C, in contrast to rHDL solely consisting of neutral or 10 mol% anionic lipids (ESI Fig. S5†). We therefore only studied rHDL based on neutral or anionic lipids (99% of the lipids).

We initially studied how the type of acyl chain of the phospholipids in the rHDL affected the association with leukocytes using rHDL containing neutral lipids, *i.e.* DMPC (contains two saturated C14 acyl chains), DPPC (contains two saturated C16 acyl chains) and POPC (contains one saturated C16 acyl chain and one unsaturated C18 acyl chain). As these lipids have the same head group (PC), we expect them to be similarly charged, thus allowing us to study the effect of the acyl chain. All the used rHDL formulations clearly associate preferentially with

monocytes over granulocytes and lymphocytes, as evident from the shifted histograms representing fluorescence intensity of DiO (Fig. 4A) and the adjusted MFI (Fig. 4B). A minor shift in the histograms and corresponding increase in MFI are seen for the granulocytes, thus indicating that some rHDL are associated with these cells. The MFI is even lower for the lymphocytes, hence, only a relatively low amount of rHDL apparently associate with the lymphocytes. Interestingly, isolated regulatory T cells (Tregs) have been reported to take up endogenous HDL to a much higher extent than other types of T cells.[41] Hence, it might be specific cell types such as Tregs that are responsible for the minor shift we do observe for the lymphocytes. However, overall it still seems to be a minor amount of the rHDL that are associated with the lymphocytes. Furthermore, although the observed preferential monocyte association seems independent of the acyl chain of the lipids in the rHDL, the MFI for the
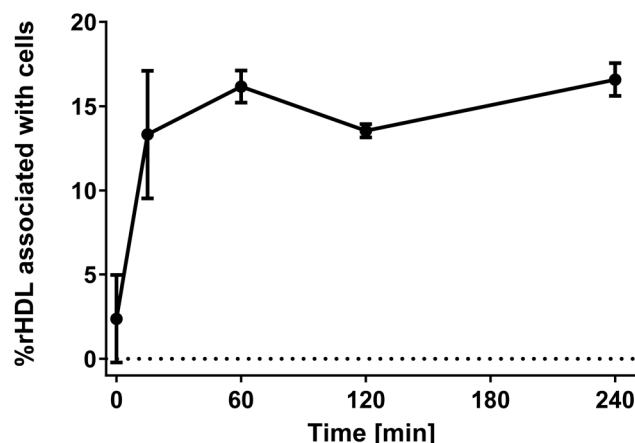

Fig. 3 The degree of rHDL association with blood cells over time showing that ~15% rHDL associate with both leukocytes and erythrocytes during four hours of incubation, which is consistent with the relatively long circulation half-life of rHDL. The experiments were conducted for DPPC:DiR 99:1 rHDL. The data represent mean ± SEM from two experiments using HWB from different donors.
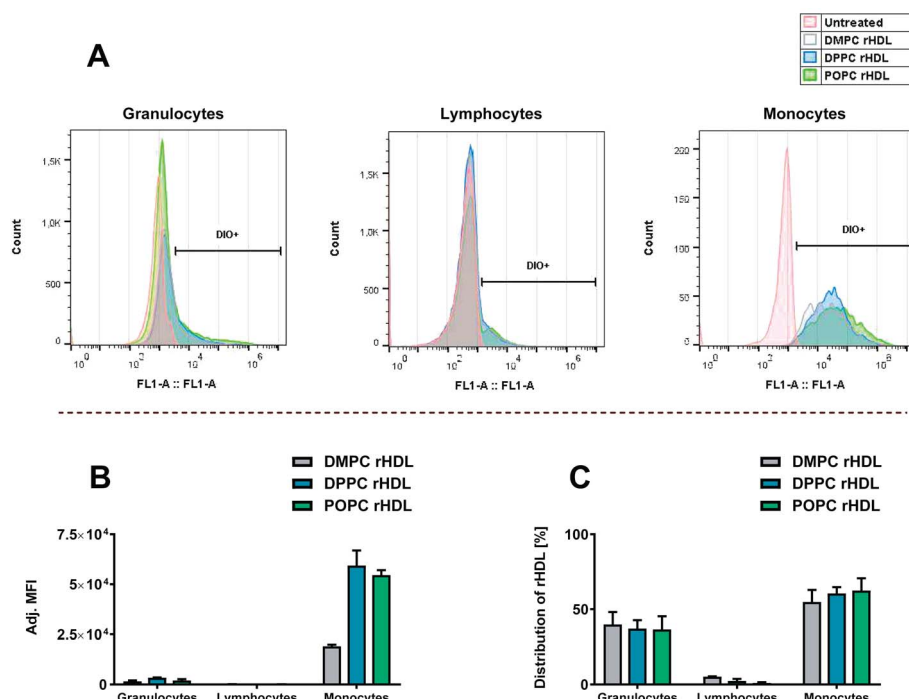
Fig. 4 The association of rHDL with leukocytes in HWB assessed by flow cytometry detecting the fluorophore label (DiO) incorporated in the rHDL. (A) Histograms representing fluorescence intensity of DiO for each type of leukocytes for one of the donors. (B) The MFI for each cell type, subtracted background and adjusted by the integral of DiO absorbance from the SEC analysis for each rHDL formulation. (C) Distribution of leukocyte-associated rHDL, obtained using the eqn (1). The data in B and C represent mean + SEM from two experiments using HWB from different donors.
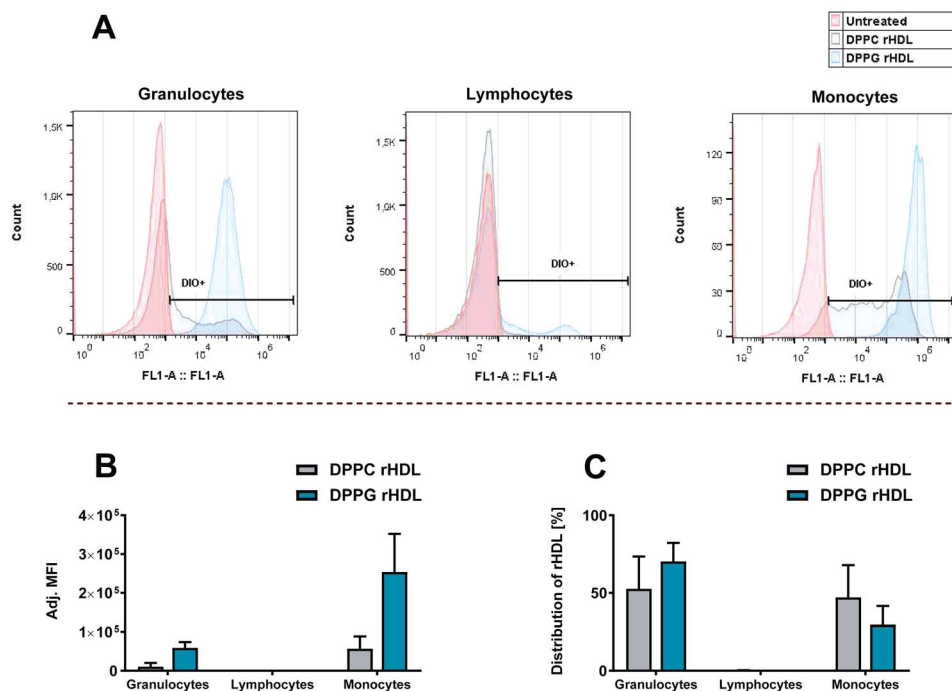
Fig. 5 The association of DPPC:DiO 99:1 rHDL and DPPG:DiO 99:1 rHDL with leukocytes assessed by flow cytometry detecting the fluorophore label (DiO) incorporated in the rHDL. (A) Histograms representing fluorescence intensity of DiO for each type of leukocytes for one of the donors. (B) The MFI for each cell type, subtracted background and adjusted by the integral of DiO absorbance from the SEC analysis for each rHDL formulation. (C) Distribution of leukocyte-associated rHDL obtained using the eqn (1). The data in B and C represent mean + SEM from two experiments using HWB from different donors.

monocytes are approximately three-fold lower when using DMPC rHDL compared to when using DPPC and POPC rHDL (Fig. 4B). We have recently shown that the dynamics of DMPC rHDL differs from DPPC and POPC rHDL, since they do not size-remodel when exposed to serum,[33] and this phenomenon might explain the lower MFI of DMPC rHDL, *i.e.* the monocytes might preferentially associate with the size-remodeled rHDL. However, the DMPC rHDL still associate preferentially with monocytes over other leukocytes, thus, the lower MFI simply indicates that lower amount of DMPC rHDL are associated with leukocytes relative to the DPPC and POPC rHDL. The preferential monocyte association of rHDL with neutral lipids stands in stark contrast to the effect observed for liposomes, where a cationic charge is required to achieve similar effects.[11]

Typically, only the MFI or percentage of positive cells are considered when studying particle uptake in leukocytes.[11,42] However, considering the distribution of rHDL in the DiO positive cells, obtained by eqn (1), which also takes the number of each cell type into account (Fig. 4C), it is evident that due to the relative higher abundance of granulocytes, the leukocyte-associated rHDL are distributed approximately equally between granulocytes and monocytes. Hence, the preferential monocytes association merely means that it is more likely that the rHDL/rHDL cargo remain associated with the cell during an encounter with a monocyte than during an encounter with a granulocyte, though the likelihood that the rHDL cargo ends up in either a monocytes or granulocyte is approximately equal. That said, even though there is an equal chance of rHDL-associated drugs to get delivered to granulocytes compared to monocytes, the relative low drug concentration in each granulocyte may be below the minimum effective concentration, thus resulting in no effect on the granulocytes.

We also investigated the effect of increasing the anionic charge of the lipid bilayer of the rHDL using DPPC (zwitterionic) and DPPG (anionic) rHDL (Fig. 5). We did observe a preferential

monocyte association for both DPPC and DPPG rHDL, as seen by the shifted chromatograms (Fig. 5A) and adjusted MFI (Fig. 5B), however, clearly the DPPG rHDL were associated to a much higher extent to the granulocytes and monocytes than the DPPC rHDL. Even though the rHDL with neutral lipid composition still have anionic charge due to the net charge on the apoA-I,[43] the higher MFI of rHDL with anionic lipid composition could be explained by the fact that phagocytic cells, including monocytes, preferably take up anionically charged particles rather than neutral particles.[18] Interestingly, though the DPPG rHDL result in relatively high MFI from the monocytes, the preferential monocyte association is not increased for DPPG rHDL relative to DPPC rHDL. This is evident from the average ratio between MFI for the monocyte and granulocytes, which is ~13.6 for DPPC rHDL and ~5.04 for DPPG rHDL, as well as the distribution of rHDL (Fig. 5C), which shows lower percentage of the DPPG rHDL associated with monocyte relative to the DPPC rHDL. These results imply that rHDL with anionic lipid composition are taken up by leukocytes (both monocytes and granulocytes) to a higher extent than rHDL with neutral lipid composition, and therefore would be cleared more rapidly from circulation than rHDL with neutral lipid composition.

The finding that rHDL associate with monocytes might seem a bit puzzling from a biological perspective, since we would not expect that endogenous HDL are cleared by monocytes. Part of this explanation may lie in the different composition of rHDL compared to HDL, as we show that the lipid composition affects to what extent the rHDL associate with leukocytes. Furthermore, as we estimated the degree of rHDL association with leukocytes to be relatively low (Fig. 3), we stress that much of the rHDL are likely not associated to any leukocytes.

It is well-established that the SR-BI can recognise rHDL and mediate uptake of rHDL cargo,[27] hence, different SR-BI expression between the different types of leukocytes could explain the preferential monocyte association. We studied the expression of SR-BI on the different types of leukocytes (Fig. 6). We do indeed
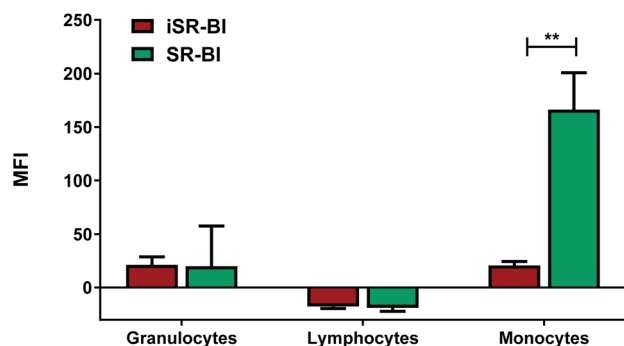

Fig. 6 The expression of SR-BI on leukocytes estimated using a specific anti-SR-BI antibody and an isotype (iSR-BI) as control. An untreated sample was used to estimate the background from each leukocyte type, which was subtracted each measurement. Note that this resulted in a slight negative MFI for the lymphocytes. Only the monocytes seemingly express SR-BI as indicated by the significantly higher MFI of the anti-SR-BI antibody relative to the iSR-BI. The data represent mean + SEM ($n = 3$). iSR-BI and SR-BI were compared with a two-way ANOVA, **, $p < 0.0011$.
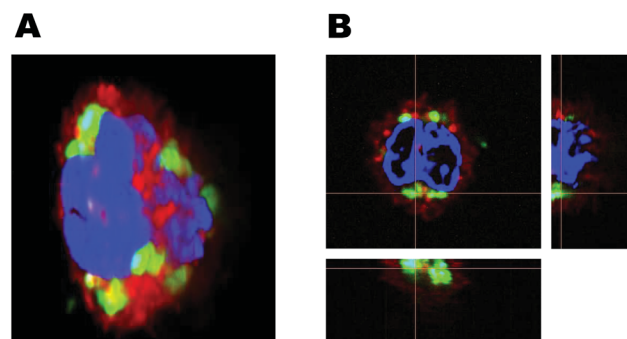

Fig. 7 Three-dimensional fluorescence microscopy for studying internalization of rHDL cargo. The anti-CD14 antibody is used to identify the surface of monocytes (red), the nucleus is stained with Hoechst (blue) and the DiO represents rHDL cargo (green). (A) Reconstructed 3D image of a monocyte with internalized DiO. (B) 2D image of a monocyte with orthogonal projection of the indicated slices, which clearly confirms the internalization of DiO.
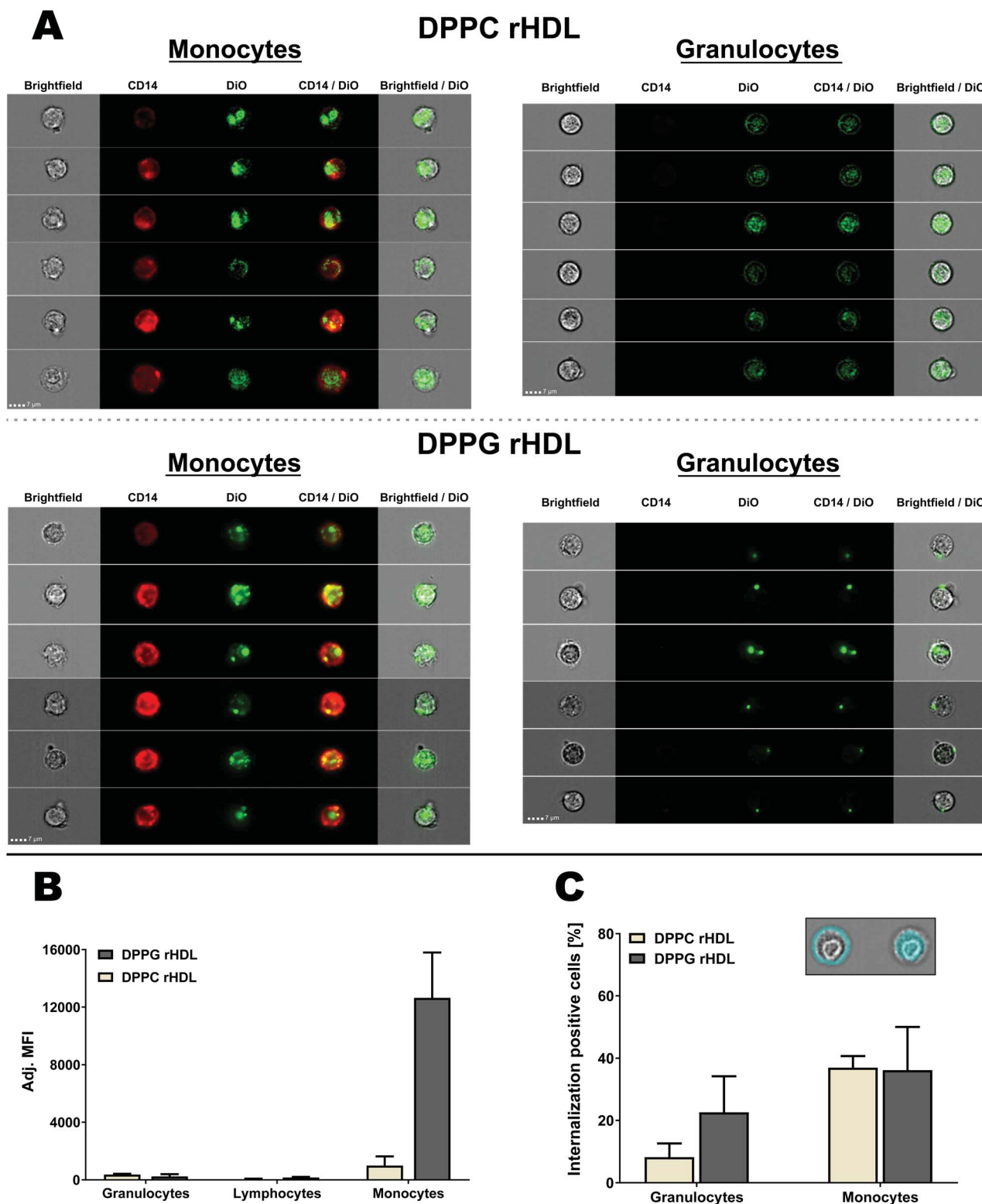
Fig. 8 Analysis of rHDL interaction with leukocytes using imaging flow cytometry for both DPPC and DPPG rHDL. (A) Selected DiO positive cells from two donors shown with brightfield (Ch01), CD14 (Ch11), DiO (Ch02), CD14/DiO and brightfield/DiO. The same contrast settings were used for monocytes and granulocytes for each of the rHDL formulations. (B) The imaging flow cytometry confirmed the preferred monocyte association of rHDL. The MFI was subtracted background from the specific cell type and adjusted by the integral of DiO absorbance from the SEC analysis of each rHDL formulation. (C) The brightfield images were used to define masks that defined the interior or the cells, as illustrated for a single monocyte in the inset, which also shows a mask of the cell surface. This allowed for the determination of the internalization of rHDL cargo, which showed more internalization positive monocytes than granulocytes. The data in B and C represent mean + SEM ($n = 2$).

obverse SR-BI expression of the monocytes, consistent with what is reported elsewhere,[28,29] however, we do also show that the SR-BI is expressed to higher extent on monocytes than the other leukocyte populations. Neither granulocytes nor lymphocytes seem to express detectable amount of SR-BI, hence, the rHDL association with granulocytes, as especially seen for DPPG rHDL, must be mediated by other mechanisms. Although, it has been reported that Tregs do express SR-BI,[41] we were not able to detect SR-BI on lymphocytes, possibly because they only account for a minor amount of the total lymphocytes. We stress that the increased SR-BI expression on monocytes might not be the only explanation for the preferential monocyte association, though it clearly seems likely that it has a significant effect.

Most drugs loaded into the rHDL for drug delivery are likely only active when internalized into the cells, however, we cannot assess from the conventional flow cytometry results if the rHDL are internalized or only adhere to the cell surface. To characterize this essential aspect of the rHDL interaction with leukocytes, we first imaged the internalization in monocytes using three-dimensional fluorescence microscopy (Fig. 7). As the rHDL cargo (DiO) was detected underneath the surface (defined by the CD14 monocyte surface marker), it clearly indicated internalization of rHDL into the monocytes. This method is obviously qualitative and to investigate the internalization more quantitatively, we used imaging flow cytometry. The imaging flow cytometry can be utilized to localize and map the cellular distribution of fluorescently labelled molecules, *e.g.* peptides, protein, nucleic acids or drugs,[44] and we here used it to characterize the internalization of rHDL in monocytes and granulocytes (Fig. 8A). We used side scatter (darkfield) and CD14 staining to identify the different type of cells (see gating strategy in ESI Fig. S2†). The imaging flow cytometry both confirmed the preferential monocyte association of DPPC and DPPG rHDL and the higher degree of association of DPPG rHDL relative to DPPC rHDL (Fig. 8B), as observed when using conventional flow cytometry (Fig. 5B).

Both monocytes and granulocytes seemingly internalize rHDL cargo (DiO) (Fig. 8A), however, many of the DPPC rHDL associated with granulocytes also cover the surface in contrast to the DPPC rHDL associated with the monocytes. The DPPG rHDL associated with the granulocytes mainly seem to reside on the surface but appear as single clusters. To be able to determine the degree of rHDL cargo (DiO) internalization in both monocytes and granulocytes, we used the brightfield images to define the interior of the cell and considered DiO measured herein as internalized (Fig. 8C, inset). Obviously, we cannot distinguish between DiO signal at the inside the cell and the center surface, *e.g.* the single clusters appearing for DPPG rHDL (Fig. 8A) seem mainly to be associated with the surface with one exception that likely are also at the surface but interpreted by the method to be internalized. Thus, the determined internalization (Fig. 8C) can be regarded as a minimum estimate. The rHDL are apparently internalized more in monocytes (average internalization positive cells of ∼37% for DPPC rHDL and ∼36% for DPPG rHDL) than in granulocytes (average internalization positive cells of ∼8.3% for DPPC rHDL and ∼23% for

DPPG rHDL), which is consistent with the observations from the images. This applies both for DPPC and DPPG rHDL, although a larger variation, and consequently a less pronounced difference, is observed for the DPPG rHDL. The higher internalization of rHDL cargo in monocytes relative to granulocytes is potentially caused by the increased SR-BI expression on monocytes (Fig. 6). However, we emphasize that more detailed studies are needed for unambiguous conclusions on the exact uptake mechanisms, though it clearly appears as there are some mechanistically differences between the rHDL association/uptake in monocytes and granulocytes.

The observed relatively high internalization of rHDL cargo in monocytes confirms that drug-loaded rHDL can deliver its drugs into the monocytes, where they can exert their therapeutic function, thus potentially leading to off-target side-effect. On the other hand, this highlights that rHDL indeed can deliver drugs into the monocytes if used for immunotherapeutic strategies relying on monocyte targeting.

Conclusions

When designing novel nanoparticle-based drug delivery systems, it is essential to establish the interactions between the nanoparticles and the immune cells either to avoid or promote an immune response. Here, we have demonstrated that rHDL preferentially associate with monocytes over other leukocytes in HWB, resulting in rHDL cargo internalization into the monocytes. We found that the association of rHDL with leukocytes could be affected by the rHDL composition (acyl chain and charge of lipids), which can be used either to increase the leukocyte association or limit it. However, using a simple quantitative approach we also showed that it was only a relatively low amount of the DPPC rHDL that did associate with the blood cells after four hours, consistent with the relatively long circulation half-life of rHDL.

Nevertheless, the association of rHDL with monocytes seems to be an inherent feature of apoA-I based rHDL, possibly mediated partly by the SR-BI on monocytes, and one has to be aware of this phenomenon, when designing rHDL for systemic drug delivery systems. It might lead to severe off-targets side-effects, when using drugs that are not intended to be taken up by leukocytes, or, on the other hand, be utilized for novel immunotherapeutic strategies aiming to deliver therapeutics to the monocytes. Furthermore, the preferential monocyte association of rHDL likely also apply for other monocyte-derived cells in tissues which could be used for a variety of immunotherapeutic strategies.

Importantly, this work also presents non-traditional methods for quantifying and characterizing the interactions between nanoparticles and cells. Conventional flow cytometry has become a popular method for studying cellular uptake of drug delivery systems, however, this method is limited by its inability (i) to quantify the proportion of the total amount of rHDL associated to the cells and (ii) to verify whether the rHDL/cargo is associated with the cell surface or internalized. Here we present approaches to provide these missing aspects. We quantified the amount of rHDL cargo/lipid-fluorophore that

were not associated with the cells from the fluorescence of the supernatant after centrifuging the cells down, and we used imaging flow cytometry to determine the degree of rHDL internalization. These quantitative methods could indeed also be applicable for studying interactions between other types of nanoparticles and cells.

Conflicts of interest

There are no conflicts to declare.

Acknowledgements

Notes and references

1 B. S. Zolnik, Á. González-Fernández, N. Sadrieh and M. A. Dobrovolskaia, *Endocrinology*, 2010, **151**, 458–465.
2 D. F. Moyano, M. Goldsmith, D. J. Solfiell, D. Landesman-Milo, O. R. Miranda, D. Peer and V. M. Rotello, *J. Am. Chem. Soc.*, 2012, **134**, 3965–3967.
3 N. M. La-Beck and A. A. Gabizon, *Front. Immunol.*, 2017, **8**, 1–6.
4 P. Mishra, B. Nayak and R. Dey, *Asian J. Pharm. Sci.*, 2016, **11**, 337–348.
5 J. Conniot, J. M. Silva, J. G. Fernandes, L. C. Silva, R. Gaspar, S. Brocchini, H. F. Florindo and T. S. Barata, *Front. Chem.*, 2014, **2**, 1–27.
6 S. Hamdy, O. Molavi, Z. Ma, A. Haddadi, A. Alshamsan, Z. Gobti, S. Elhasi, J. Samuel and A. Lavasanifar, *Vaccine*, 2008, **26**, 5046–5057.
7 W. Martinet, S. Verheye and G. R. Y. D. Meyer, *Trends Cardiovasc. Med.*, 2007, **17**, 69–75.
8 C. L. van Broekhoven, C. R. Parish, C. Demangel, W. J. Britton and J. G. Altin, *Cancer Res.*, 2004, **64**, 4357–4365.
9 W. C. Chen, N. Kawasaki, C. M. Nycholat, S. Han, J. Pilotte, P. R. Crocker and J. C. Paulson, *PLoS One*, 2012, **7**, e39039.
10 D. Schmid, C. G. Park, C. A. Hartl, N. Subedi, A. N. Cartwright, R. B. Puerto, Y. Zheng, J. Maiarana, G. J. Freeman, K. W. Wucherpfennig, D. J. Irvine and M. S. Goldberg, *Nat. Commun.*, 2017, **8**, 1–12.
11 P. T. Johansen, D. Zucker, L. Parhamifar, H. Pourhassan, D. V. Madsen and J. R. Henriksen, *Expert Opin. Drug Delivery*, 2015, **12**, 1045–1058.
12 C. Shi and E. G. Pamer, *Nat. Rev. Immunol.*, 2011, **11**, 762–774.
13 F. Leuschner, P. Dutta, R. Gorbatov, T. I. Novobrantseva, J. S. Donahoe, G. Courties, K. M. Lee, J. I. Kim, J. F. Markmann, B. Marinelli, P. Panizzi, W. W. Lee, Y. Iwamoto, S. Milstein, H. Epstein-Barash, W. Cantley, J. Wong, V. Cortez-Retamozo, A. Newton, K. Love, P. Libby, M. J. Pittet, F. K. Swirski, V. Koteliansky, R. Langer, R. Weissleder, D. G. Anderson and M. Nahrendorf, *Nat. Biotechnol.*, 2011, **29**, 1005–1013.
14 E. Cohen-Sela, O. Rosenzweig, J. Gao, H. Epstein, I. Gati, R. Reich, H. D. Danenberg and G. Golomb, *J. Controlled Release*, 2006, **113**, 23–30.
15 B. Schumak, K. Klocke, J. M. Kuepper, A. Biswas, A. Djie-Maletz, N. van Rooijen, M. Mack, A. Hoerauf and I. R. Dunay, *PLoS One*, 2015, **10**, e0124080.
16 C. Kelly, C. Jefferies and S.-A. Cryan, *J. Drug Delivery*, 2011, **2011**, 1–11.
17 G. Lauvaua, P. Loke and T. M. Hohl, *Semin. Immunol.*, 2015, **27**, 397–409.
18 E. Fröhlich, *Int. J. Nanomed.*, 2012, **7**, 5577–5591.
19 H. Epstein-Barash, D. Gutman, E. Markovsky, G. Mishan-Eisenberg, N. Koroukhov, J. Szebeni and G. Golomb, *J. Controlled Release*, 2010, **146**, 182–195.
20 H. Lv, S. Zhang, B. Wang, S. Cui and J. Yan, *J. Controlled Release*, 2006, **114**, 100–109.
21 R. Kuai, L. J. Ochyl, K. S. Bahjat, A. Schwendeman and J. J. Moon, *Nat. Mater.*, 2017, **16**, 489–496.
22 M. Rui, Y. Xin, R. Li, Y. Ge, C. Feng and X. Xu, *Mol. Pharmaceutics*, 2017, **14**, 107–123.
23 J. Wang, J. Jia, J. Liu, H. He, W. Zhang and Z. Li, *Drug Delivery*, 2013, **20**, 356–363.
24 J. B. Simonsen, *Nanomedicine*, 2016, **12**, 2161–2179.
25 R. Kuai, D. Li, Y. E. Chen, J. J. Moon and A. Schwendeman, *ACS Nano*, 2016, **10**, 3015–3041.
26 A. L. Catapano, A. Pirillo, F. Bonacina and G. D. Norata, *Cardiovasc. Res.*, 2014, **103**, 372–383.
27 W.-J. Shen, S. Azhar and F. B. Kraemer, *Annu. Rev. Physiol.*, 2018, **80**, 95–116.
28 M. C. Roque-Cuéllar, B. Sánchez, J. R. García-Lozano, A. Garrido-Serrano, M. Sayago, J. M. Praena-Fernández, A. Núñez-Roldán and J. Aguilar-Reina, *J. Med. Virol.*, 2012, **84**, 1727–1736.
29 H. Barth, E. K. Schnober, C. Neumann-Haefelin, C. Thumann, M. B. Zeisel, H. M. Diepolder, Z. Hu, T. J. Liang, H. E. Blum, R. Thimme, M. Lambotin and T. F. Baumert, *J. Virol.*, 2008, **82**, 3466–3479.
30 K. N. Liadaki, T. Liu, S. Xu, B. Y. Ishida, P. N. Duchateaux, J. P. Krieger, J. Kane, M. Krieger and V. I. Zannis, *J. Biol. Chem.*, 2000, **275**, 21262–21271.
31 A. Rigotti, S. L. Acton and M. Krieger, *J. Biol. Chem.*, 1995, **270**, 16221–16224.
32 J. Tanga, S. Baxter, A. Menon, A. Alaarg, B. L. Sanchez-Gaytan, F. Fay, Y. Zhao, M. Ouimet, M. S. Braza, V. A. Longo, D. Abdel-Atti, R. Duivenvoorden, C. Calcagno, G. Storm, S. Tsimikas, K. J. Moore, F. K. Swirski, M. Nahrendorf, E. A. Fisher, C. Pĕrez-Medina, Z. A. Fayad, T. Reiner and W. J. M. Mulder, *Proc. Natl. Acad. Sci. U. S. A.*, 2016, **113**, E6731–E6740.
33 D. Pedersbæk, M. K. Kræmer, J. Ashley, S. Braesch-Andersen, T. L. Andresen and J. B. Simonsen, *Bioconjugate Chem.*, 2019, **30**, 2634–2646.
34 A. Jonas, *Methods Enzymol.*, 1986, **128**, 553–582.

35 M. R. Whorton, B. Jastrzebska, P. S.-H. Park, D. Fotiadis, A. Engel, K. Palczewski and R. K. Sunahara, *J. Biol. Chem.*, 2008, **283**, 4387–4394.

36 M. Wadsäter, S. Maric, J. B. Simonsen, K. Mortensen and M. Cardenas, *Soft Matter*, 2013, **9**, 2329–2337.

37 S. H. Kuhn, B. Gemperli, E. G. Shephard, J. R. Joubert, P. A. C. Weidemann, G. Weissmann and M. C. Finkelstein, *Biochim. Biophys. Acta*, 1983, **762**, 119–127.

38 R. Münter, K. Kristensen, D. Pedersbæk, J. B. Larsen, J. B. Simonsen and T. L. Andresen, *Nanoscale*, 2018, **10**, 22720–22724.

39 J. B. Simonsen, *J. Extracell. Vesicles*, 2019, **8**, 1582237.

40 V. Ost, J. Neukammer and H. Rinneberg, *Cytometry*, 1998, **32**, 191–197.

41 C. M. Rueda, A. L. Rodríguez-Perea, M. Moreno-Fernandez, C. M. Jackson, J. T. Melchior, W. S. Davidson and C. A. Chougnet, *J. Lipid Res.*, 2017, **58**, 1514–1523.

42 E. Karathanasis, C. M. Geigerman, C. A. Parkos, L. Chan, R. V. Bellamkonda and D. L. Jaye, *Ann. Biomed. Eng.*, 2009, **37**, 1984–1992.

43 D. L. Sparks, S. Lund-Katz and M. C. Phillips, *J. Biol. Chem.*, 1992, **267**, 25839–25847.

44 M. Doan, I. Vorobjev, P. Rees, A. Filby, O. Wolkenhauer, A. E. Goldfeld, J. Lieberman, N. Barteneva, A. E. Carpenter and H. Hennig, *Trends Biotechnol.*, 2018, **36**, 649–652.